Novel Class of Crystal/Glass Ultrafine Nanolaminates with Large and Tunable Mechanical Properties

Francesco Bignoli, Philippe Djemia, Giancarlo Terraneo, Grégory Abadias, Christoph Gammer, Alice Lassnig, Camila Teixeira, Subin Lee, Ali Ahmadian, Andrea Li Bassi, et al.

Novel class of crystal/glass ultrafine nanolaminates with large and tunable mechanical properties

Francesco Bignoli[a,b], Philippe Djemia[a], Giancarlo Terraneo[c], Gregory Abadias[d], Christoph Gammer[e], Alice Lassnig[e], Camila A. Teixeira[f], Subin Lee[f], Ali Ahmadian[g], Andrea Li Bassi[b], Damien Faurie[a], Matteo Ghidelli[a]**

[a]*Laboratoire des Sciences des Procédés et des Matériaux (LSPM), CNRS, Université Sorbonne Paris Nord, 93430, Villetaneuse, France*

[b]*Dipartimento di Energia, Laboratorio Materiali Micro e Nanostrutturati, Politecnico di Milano, via Ponzio 34/3, I-20133 Milano, Italy*

[c]*Laboratory of Supramolecular and Bio-Nanomaterials (SupraBioNanoLab), Department of Chemistry, Materials, and Chemical Engineering "Giulio Natta", Politecnico di Milano, Milano, 20131, Italy*

[d]*Institut Pprime, UPR 3346, CNRS-Université de Poitiers-ENSMA, 11 Boulevard Marie et Pierre Curie, 86073 Poitiers Cedex 9, France*

[e]*Erich Schmid Institute of Materials Science, Austrian Academy of Sciences, Jahnstrasse 12, 8700 Leoben, Austria*

[f]*Institute for Applied Materials, Karlsruhe Institute of Technology, 76344, Eggenstein-Leopoldshafen, Germany*

[g]*INT Institute of Nanotechnologies, Karlsruhe Institute of Technology, 76344, Eggenstein-Leopoldshafen, Germany*

*Email: francesco.bignoli@lspm.cnrs.fr, matteo.ghidelli@lspm.cnrs.fr

Keywords:

Amorphous/crystalline nanolaminates; metallic glasses; local heterogeneities; pulsed laser deposition; scale-bridge structural-mechanical characterizations.

Abstract

The control of local heterogeneities in metallic glasses (MGs) represents an emerging field to improve their plasticity, preventing the propagation of catastrophic shear bands (SBs) responsible for the macroscopically brittle failure. To date, a nanoengineered approach aimed at finely tuning local heterogeneities controlling SB nucleation and propagation is still missing, hindering the potential to develop MGs with large and tunable strength/ductility balance and controlled deformation behavior. In this work, we exploited the potential of pulsed laser deposition (PLD) to synthesize a novel class of crystal/glass ultrafine nanolaminates (U-NLs) in which a ~4 nm thick crystalline Al separates 6 and 9 nm thick Zr50Cu50 glass nanolayers, while reporting a high density of sharp interfaces and large chemical intermixing. In addition, we tune the morphology by synthesizing compact and nanogranular U-NLs, exploiting, respectively, atom-by-atom or cluster-assembled growth regimes. For compact U-NLs, we report high mass density (~8.35 g/cm3) and enhanced and tunable mechanical behavior, reaching maximum values of hardness and yield strength of up to 9.3 and 3.6 GPa, respectively. In addition, we show up to 3.6% homogeneous elastoplastic deformation in compression as a result of SB blocking by the Al-rich sublayers. On the other hand, nanogranular U-NLs exhibit slightly lower yield strength (3.4 GPa) in combination with enhanced elastoplastic deformation (~6%) followed by the formation of superficial SBs, which are not percolative even at deformations exceeding 15%, as a result of the larger free volume content within the cluster-assembled structure and the presence of crystal/glass

nanointerfaces, enabling to accommodate SB events. Overall, we show how PLD enables the synthesis of crystal/glass U-NLs with ultimate control of local heterogeneities down to the atomic scale, providing new nanoengineered strategies capable of deep control of the deformation behavior, surpassing traditional trade-off between strength and ductility. Our approach can be extended to other combinations of metallic materials with clear interest for industrial applications such as structural coatings and microelectronics (MEMS and NEMS).

1. Introduction

Metallic glasses (MGs) are amorphous materials characterized by an atomic structure lacking long range order leading to the combination of high yield strength (> 2 GPa) and elasticity (≈2%) [1]. However, in their bulk form, they deform through the formation of very thin (∼10 nm) shear bands (SBs) concentrating all shear strain localization and leading to and almost instantaneous propagation once the yield stress is exceeded, resulting in a macroscopically brittle behavior [2]. To face this issue, the control of local heterogeneities at the atomic or micro-scale has a key role, enabling a mitigation of the SB process. A first approach is represented by modifying the atomic arrangement through compositional segregation or by controlling free volume to hinder and deviate the nucleation/propagation of SBs [3, 4]. As an example, ZrCu nanoglasses [5, 6] and cluster-assembled MGs[7] show a high density of amorphous interfaces and chemical fluctuations, resulting in a higher yield strength (≥3 GPa) and ductility in tension (∼10%). The remarkable plasticity can be attributed to the formation of numerous SBs that accommodate the strain.

A second strategy aims at reducing the intrinsic size of the specimen below the micrometer scale, activating mechanical size effects, resulting in homogenous deformation because of the reduced probability to have defects acting as stress concentrators which can trigger SB process [8]. In this line, the synthesis of multilayers represents an interesting approach combining the layer confinement (size effects) with the possibility to control the local heterogeneities by tuning the chemical/structural contrast between the layers (i.e. amorphous and crystalline) together with exhibiting a high interface density. For example, ZrCu/Cu amorphous/crystalline multilayer with a bilayer period of 20 nm deforms plastically up to 10% without formation of SBs, while still having a yield strength of ∼2.4 GPa [9]. This is due to a co-deformation mechanism in which the embryonic SBs cannot reach the levels of stress required for nucleation/propagation due to the thickness confinement and the presence of the adjacent Cu layers,

while the dislocations within Cu needs more energy to propagate, resulting in an increment of the overall strength and ductility [9, 10].

However, the research on the control of local heterogeneities in MGs presents many challenges, limiting the control of the SB process and the overall mechanical behavior. For instance, an easy and fast method to deposit ultrafine nanolayered structures is lacking (sublayer thickness < 10 nm), enabling large chemical intermixing and high density of interfaces benefiting the mechanical behavior. Specifically, deposition carried out by magnetron sputtering has limitations resulting from the need of ultra-fast speed for shutters opening/closing (1 cycle every 2-10 seconds) in combination with a fast regulation of the power applied to the targets so as to produce U-NL with different chemical structure (amorphous/crystalline) [11].

Moreover, at present it is not possible to couple different nanostructuring strategies (i.e. fabrication of compact/nanogranular morphologies) within the same deposition step, preventing an advanced synthesis approach of amorphous/crystalline U-NLs with better and tunable mechanical behavior, beyond the average of their single components.

In this paper, we use pulsed laser deposition (PLD) to fabricate new $Zr_{50}Cu_{50}$/Al ultrafine nanolaminates (U-NLs) with compact or nanogranular morphologies and ultrafine bilayer period (up to 13 nm) leading to a unique combination of strength and ductility. The local structure and mechanical properties are extensively characterized by scale-bridging techniques including X-ray diffraction/reflectivity (XRD/XRR), scanning and transmission electron microscopies (SEM/TEM), optoacoustic techniques, nanoindentation and *in situ* SEM micropillar compression to precisely investigate the effects of local heterogeneities on the strength and deformation mechanisms. We show that the $Zr_{50}Cu_{50}$/Al U-NLs are stronger than magnetron sputtered (MS) ZrCu-based thin film metallic glasses (TFMGs) and multilayers, reaching a yield strength of $\sigma_y > 3.4$ GPa for compact U-NLs. Moreover, cluster-assembled nanogranular U-NLs show large homogenous deformation up to 6% (in

compression), followed by the formation of superficial SBs which do not percolate through sample even at larger deformations (>15%). Such new mechanism is revealed by TEM of the pillars after compression showing that compact U-NLs fail with shear banding, while nanogranular counterparts deform more homogenously with only superficial SBs due to the complex interplay between the enhanced free volume within crystal/glass nanoclusters and the ultrafine nanolayered structure.

2. Materials and Methods

2.1 Synthesis of $Zr_{50}Cu_{50}$/Al U-NLs with controlled bilayer period and nanostructure

$Zr_{50}Cu_{50}$ (% at.) films were deposited by ablating a $Zr_{50}Cu_{50}$ target (99.99% pure, produced by Mateck®), while the fabrication of $Zr_{50}Cu_{50}$/Al U-NLs was carried out by covering part of the target surface with Al (99.99% pure) stripes of different width to control the relative thickness of the amorphous and crystalline layers as shown in the section S1 of the supplementary information. The target was ablated with a ns-pulsed laser (Nd:YAG, 1st harmonic, λ = 1064 nm, repetition rate 10 Hz, pulse duration 5-7 ns), pulse energy equal to 1650 mJ, focused on the target to obtain a fluence of 14 J/cm^2. Si (100) was used as substrates after being cleaned in an ultrasonic bath in isopropanol. The substrates were mounted on a rotating substrate holder with a fixed distance from the target equal to 70 mm. All depositions were performed at room temperature in vacuum ($1x10^{-3}$ Pa) or under pure He atmosphere at a pressure of 5 Pa to deposit compact and cluster-assembled nanogranular U-NLs, respectively. The thickness of the U-NLs is in the order of ~800 nm, while 2 μm samples were deposited for micropillar compression tests.

The U-NLs structures were fabricated by controlling the target roto-translation and the width of the Al stripes mounted on the $Zr_{50}Cu_{50}$ in order to tune the number of the laser shots on the ablated materials, while taking into account the difference in the deposition rate between Al and $Zr_{50}Cu_{50}$, respectively, ~2 and ~1.1 nm/s. This enables a precise control of the number of shots on the $Zr_{50}Cu_{50}$ target and Al strip enabling to adjust the thickness of the amorphous layer (~55-80 shots), while keeping constant the

number of shots on the Al strips (~20 shots). This results in NL with two different periods, corresponding to Al volume fraction of 30 and 40%. TEM analysis was carried out first on selected samples to precisely determine the bilayer period of $Zr_{50}Cu_{50}$ and Al. Then, a calibration was carried out by combining both XRR and XRD data to identify the thickness of amorphous/crystalline ultrafine sublayers. This methodology has the advantage to be extremely rapid with respect to more time-consuming TEM investigations, while enabling an accurate control of the thickness single sublayers as shown in the Section 2 of the Supplementary Information. The total thickness as well as thickness of the crystalline (t_c) and amorphous (t_a) sublayers are presented in Table 1. In this study, we focus on U-NLs with a $t_a/t_c > 1$, expecting a high strength due to the larger fraction of amorphous phase, while keeping a high plasticity due to the presence of FCC Al sublayers, as expected from molecular dynamics simulations [12] and observed in ZrCu/Cu 100/50 nm multilayers ($t_a/t_c = 2$) combining a yield strength (σ_y) of 2.1 GPa and ductility around 12% [10].

	Total thickness 800 nm	**Total thickness 2 µm**
Nanolayer period [nm $Zr_{50}Cu_{50}$ /nm Al]	800/0, 6/4, 9/4	9/4

Table 1*: Crystalline/amorphous U-NLs fabricated in this work. The 800 nm U-NLs were used for the structural characterization (SEM, XRD, XRR and TEM) and mechanical characterization with optoacoustic techniques and nanoindentation, while the 2 µm U-NLs were used for the micropillar compression tests.*

2.2 Structural characterization

The crystallographic structure of the U-NLs was investigated by X-ray diffraction (XRD) using a θ-2θ Bruker D8 Advanced system with Cu Kα radiation (λ = 0.154 nm) operated in grazing incidence geometry with an incidence angle of 0.95° with a 2θ scan range 20-90°. Data were acquired overnight by Lynx Eye detector in continuous scanning mode with a 2θ step size of 0.14°.

A field emission SEM (Supra, Zeiss) 40 equipped with a Bruker energy dispersive X-ray spectroscopy (EDX) was used to perform morphological and elemental characterization of the U-NLs deposited on Si (100) substrates.

X-ray reflectivity (XRR) scans were obtained with a Seifert XRD 3000 diffractometer operating at 40 kV and 40 mA using a Cu Kα source. The scans were carried out between 0.2° and 2.2° with a step of 0.05° to determine the density of the U-NLs and estimate the period of the NL structure structures as explained in the section S2 of the supplementary.

To get high resolution information of the layered structures and elemental distribution of the as deposited nanolayered structures cross-sectional transmission electron microscopy (TEM) analyses were performed using a JEOL 2200 FS operating at 200 kV. A combination of high-angle annular dark-field scanning TEM (HAADF-STEM), selected area electron diffraction (SAED) and STEM-EDX were acquired to characterize morphology structure and chemistry at the nanoscale. The lamellae used for TEM characterization were prepared with a Ga Focused Ion Beam (FIB) with and extremely low current equal to 50 pA, while protecting the sample with a 100 nm Pt layer to minimize damaging.

For the post-mortem characterization of tested pillars, TEM and STEM-EDX was carried out in an aberration probe-corrected Thermo Fisher Titan Themis 60-300 equipped with the ChemiSTEM Super X EDX detector operated at 300 kV.

2.3 Mechanical characterization

The elastic properties of the U-NLs were extracted by Brillouin light scattering (BLS) spectroscopy and picosecond laser ultrasonics in air, as described in section S3 of the supplementary and in the references [13, 14].

The Young's modulus (E) and the hardness (H) of the U-NLs were extracted by nanoindentation by using a KLA G200 with a Berkovich diamond indenter operated in continuous stiffness measurement (CSM) mode to measure their depth profile. A standard fused silica sample was tested before and after the measurements for tip and frame stiffness calibrations. The Oliver and Pharr [15] model was applied to extract E and H at indentation depth equal to 10 % of the film thickness with a fixed load rate of 0.05 s^{-1}, thermal drift <0.05 nm/S and 25 indents for each sample. More detail can be found is section S4 of the supplementary.

Micropillar compression tests were performed on the 2 μm samples in a SEM (Merlin Gemini II, Zeiss) with a Bruker Hysitron PI89 SEM PicoIndenter (maximum force of 0.5 N and noise floor of 5 μN) equipped with a 2 μm diamond flat punch (Synthon-MDP AG) in displacement control mode with a strain rate of $10^{-2}s^{-1}$. Micropillars were machined with a gallium focus ion beam (FIB, Crossbeam 550L Zeiss) operated at an acceleration voltage of 30 kV using a 3-step process; coarse milling with a current of 7 nA, 1.5 nA for intermediate and 300 pA for fine milling. Four pillars were tested for each sample with stress obtained as force divided by the top area of the pillar. The pillars have an average diameter of 720 nm and height around 2 μm to avoid substrate interferences and the activation of mechanical size effects which increase extrinsically the yield strength and ductility of the MGs when the diameter of the tested samples goes below 300 nm [16, 17]. More details regarding the tests and how the yield strength σ_y and homogeneous deformation with their statistics were obtained can be found in the Section S5 of the supplementary.

3. Results and discussion

3.1 Atomic and microstructure of $Zr_{50}Cu_{50}$/Al U-NLs

The microstructure of compact U-NLs deposited in vacuum and of nanogranular U-NLs deposited in 5 Pa He has been investigated by SEM, XRD and TEM. The SEM cross-section (Figures 1a,b) shows the absence of macroscopic defects such as porosity and phase segregations, which could affect the mechanical behavior and the presence of corrugations, induced by the propagation of SBs typical of MGs [18]. This is expected since the t_a/t_c is > 1 leading to deformation process dominated by SBs propagation especially when performing cleavage cuts which force sharp crack propagation from Si substrate to the U-NLs [12, 18].

The XRD patterns for the compact and nanogranular *$Zr_{50}Cu_{50}$/Al U-NLs* presented in Figures 1c,d respectively, show that the pure $Zr_{50}Cu_{50}$ is completely amorphous with a main peak centered at 2θ = 37.7° as expected from literature[14]. However, the full width at half maximum (FWHM) of the nanogranular film in Figure 1d is wider (11.5°) than that of the compact film counterpart in Figure 1c (7.5°), indicating a more disordered and heterogeneous structure due to their cluster-assembled growth such as for nanoglasses [7, 19]. The U-NLs also show a peak at 2θ = 38.5° which corresponds to the (111) plane of FCC Al, indicating a textured growth of the crystalline layer. The peak is more pronounced with increased Al relative fraction. The size of the Al crystallites, obtained by Scherrer's equation on the Al (111) reflection, is ~4.0 ± 0.5 nm, see supplementary section S2 for more information.

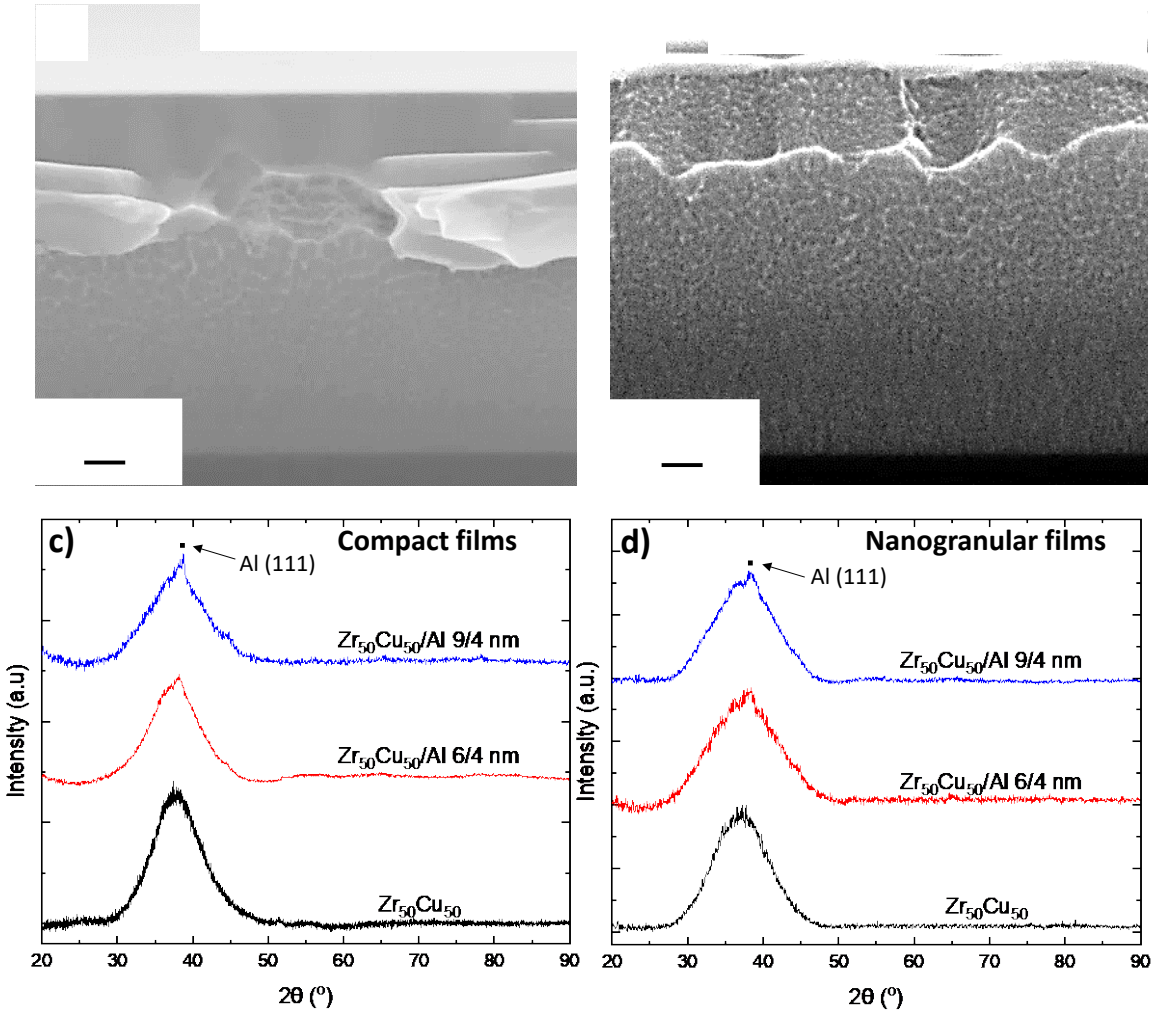

Figure 1. *Cross sectional SEM and XRD patterns as a function of bilayer period of compact (a,c) and nanogranular (b,d) $Zr_{50}Cu_{50}$/Al U-NLs, respectively.*

A more detailed investigation of the nanostructure of the U-NLs alternating 4.0 ± 0.5 nm of Al and 9.0 ± 0.5 nm of $Zr_{50}Cu_{50}$ (referred as $Zr_{50}Cu_{50}$/Al 9/4 nm) was conducted by STEM. Figures 2a,b display HAADF STEM images of compact (a) and nanogranular U-NLs (b) revealing a nanolayered structure with straight interfaces. Such structure differs from previously reported nanolaminates with similar bilayer periods (6 – 20 nm) deposited by magnetron sputtering which usually have undulating interfaces due to the incomplete coalescence of the islands during the sputtering of the single interlayers [11, 20, 21]. As a matter of facts, PLD enable larger energy of the deposited species (> 15 eV) vs magnetron sputtering

(∼1 eV) allowing a faster percolation of the islands, forming the defined interlayers with large chemical intermixing [22]. Figure 2b also shows that the single layers composing the nanogranular U-NLs are not homogenous, but formed by nano-size clusters due to the in-plume cluster formation induced by the background deposition pressure[7]. These clusters have brighter cores and darker surroundings indicating a change in the relative density from the center (denser) to the interfaces (less dense) due to chemical segregation during the cluster formation and the formation of topological defects during the bonding of adjacent clusters such as in nanoglasses [5, 6]. SAED patterns in the insets of Figures 2a,b reveal a single band in agreement with the XRD, but without spot patterns expected from the crystalline Al layers. This could be related with the elemental chemical intermixing phenomena (formation of the ZrCuAl) for both compact and nanogranular U-NLs (Figure 2c and d) as well as by the difficulty of to obtain SEAD patterns of the nanocrystalline Al, which possesses very small intrinsic sizes (≤ 4nm). The thickness of the layers estimated by HAADF STEM and STEM-EDX line profile are quite similar and can be considered equal. In both cases we show chemical intermixing between the Al and the $Zr_{50}Cu_{50}$ layers with high concentrations of Zr and Cu in the Al layers and with the peaks of Al concentrations (dash vertical lines) being in counterphase with the Cu concentration (dash – dot vertical lines) due to the low miscibility between Al and Cu ($\Delta H_{mix\ Al\text{-}Cu}$ = -1 kJ/mol) [23]. The intermixing between the layers is favored by the thin thickness of the sublayers of the U-NLs [11, 24], the high mixing enthalpy between Zr and Al ($\Delta H_{mix\ Zr\text{-}Al}$ = *-44 kJ/mol)* [23], the high reactivity of the Al nanocrystalline grain boundaries [25] and the high surface mobility of the atoms during the film growth due to the high energies of PLD [22]. This chemical diffusion of Al and ZrCu between the different sublayers generate a ZrCuAl phase with interatomic distance close to $Zr_{50}Cu_{50}$ (2.5 Å) [13]. However, a more accurate analysis using techniques such as atom probe tomography (APT) will be necessary to achieve higher spatial resolution, especially for the case of U-NLs with nm-sized bilayer periods explored in this study. The SAED signal of this new phase would then reduce the intensity of the SAED of the base components such as in TiAl intermetallics grown

during the annealing of Al/Ti multilayers [26]. The formation of the ZrCuAl phase slightly reduce the effective thickness of the crystalline layer (t_c), consequentially increasing the t_a/t_c ratio which, however, remains >1. This results in comparable mechanical properties and deformation behavior as shown in Ref. [12], which focuses on with molecular dynamic (MD) simulations investigating the effect of bilayer period for crystalline/amorphous nanolaminates.

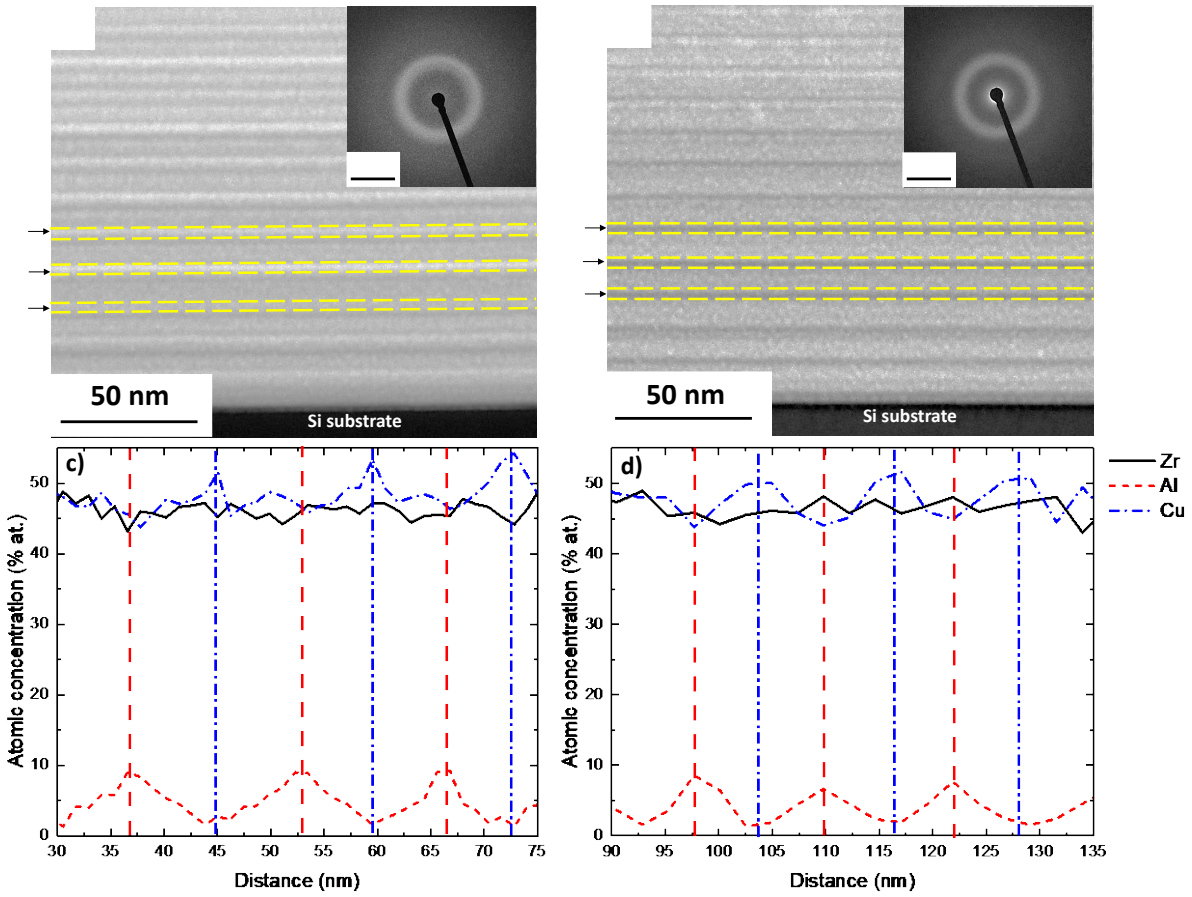

Figure 2. *HAADF-STEM images of compact (a) and nanogranular (b) $Zr_{50}Cu_{50}$/Al U-NLs showing the nanolayered microstructure with $Zr_{50}Cu_{50}$ layer thickness of 9.0 ± 0.5 separated by 4.0 ± 0.5nm Al layers. The corresponding SAED pattern in the inset of a) and b) highlight mainly the amorphous structure of both samples. The averaged STEM-EDX line profiles across several layers for both compact (c) and nanogranular (d) U-NLs shows a large intermixing between the nanolayers.*

Figure 3 shows the evolution of the mass density for U-NLs compared to magnetron sputtered (MS) deposited ZrCu films [13, 27]. Firstly, the nanogranular U-NLs are slightly less dense than their compact counterparts due to the higher amount of free volume originated by the cluster-assembled growth[7]. Moreover, the density of compact $Zr_{50}Cu_{50}$ PLD films (8.35 g/cm^3) is at least 10% higher than their traditional MS counterparts (7.4 g/cm^3) [13, 27]. This phenomenon, already observed in literature for oxides [28] and carbon films [29], is related to the high fluence used in PLD which confers higher amounts of kinetic energy to the atoms in the plasma plume allowing the growth of films with a more closely packed atomic structure [22]. Lastly, for both compact and nanogranular nanolaminates, the density decreases with increasing the Al volume fraction (an element with lower mass density) varying from 8.35 and 7.98 g/cm^3 for compact and nanogranular $Zr_{50}Cu_{50}$ down to 7.9 and 7.6 g/cm^3 for the corresponding U-NLs alternating 4 nm of Al and 6 nm of $Zr_{50}Cu_{50}$. However, such values are still higher than the density of MS $Zr_{50}Cu_{50}$ with 7.4 g/cm^3 even considering a 40% Al volume fraction within the PLD deposited U-NLs. This can be explained by the high energies of PLD and high chemical intermixing between the Al and $Zr_{50}Cu_{50}$ layers forming a denser ZrCuAl amorphous phase (~7.1 g/cm^3) [13, 27] than pure Al (2.7 g/cm^3) [30]. This result reduces the drop in density that could be expected for high volume fractions of pure Al.

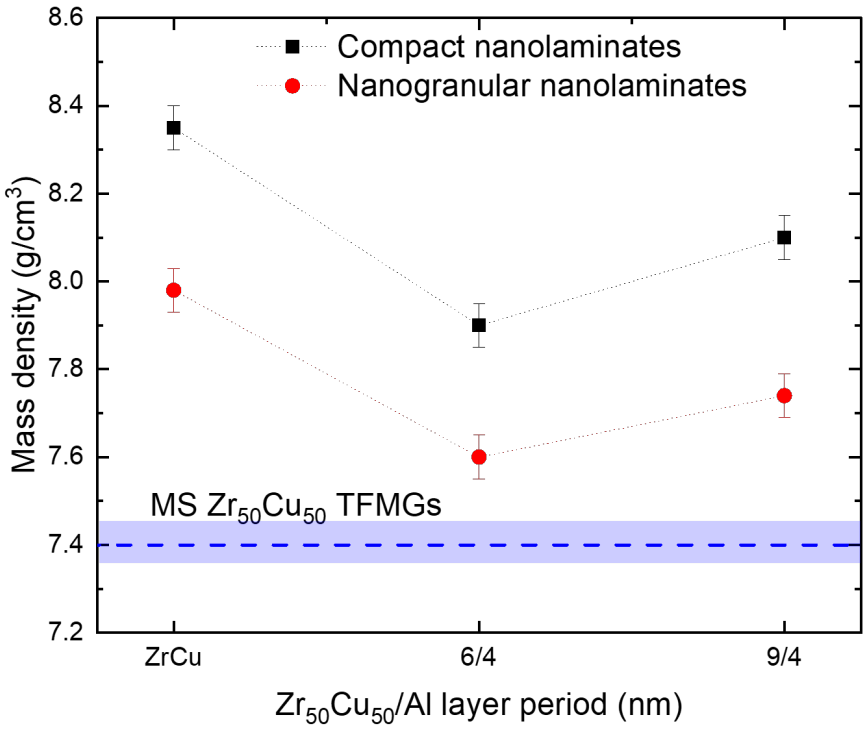

Figure 3. *Evolution of the mass density of compact and nanogranular $Zr_{50}Cu_{50}$/Al U-NLs with different layered structure.*

3.2 Mechanical properties of $Zr_{50}Cu_{50}$/Al U-NLs

Figure 4 presents the evolution of the Young's modulus (*E*) obtained by optoacoustic techniques and nanoindentation and hardness (*H)* obtained by nanoindentation. Both compact and nanogranular U-NLs follow the same trend and have similar values of *E* and *H* as a function of the layer period indicating that the transition from compact to nanogranular morphology has only a minor effect on the elastic properties of the U-NLs. This is probably due to the fact that elastic constants are essentially linked to structure (at the bond scale), rather than microstructure. The small (7%) difference between the elastic modulus measured by nanoindentation and the one measured by optoacoustic techniques is related to substrate effects present during nanoindentation [31] and have already been observed in other works [13, 14]. Furthermore, we observe that *E* and *H* of our PLD deposited films are much higher (30%) than those of sputter-deposited ZrCu TFMGs [14, 32] and similar multilayers [9, 10]. This results from the higher density of

the PLD films as observed in the W and W-O films deposited with different densities by Besozzi *et al*. [33, 34] in which the increase of the elastic moduli is directly proportional to the densification of the films.

The introduction of the Al nanolayering increases *E* and *H* from 120 and 8.6 GPa of $Zr_{50}Cu_{50}$ up to 139 and 9.3 GPa for the corresponding U-NLs with $Zr_{50}Cu_{50}$/Al 9/4 nm. This value is higher than the theoretical average of *E* and *H* of the single $Zr_{50}Cu_{50}$ and Al layers based on the relative volume fraction of Al, namely 105 and 6.4 GPa, because of the formation of a U-NL structure. However, such trend is opposite to what observed in the literature of amorphous/crystals multilayers reporting decrement of *H* for larger fraction of the FCC crystalline phase such as in the case of ZrCu/Cu multilayers [10, 35] which show a reduction of *H* down 5.9 GPa for 50% Cu volume fraction. The behavior observed of U-NLs can be related to a combination of many factors among which the high density of crystalline/amorphous interfaces, which have been demonstrated to increase the mechanical strength of the structure [24] since the interfaces can confine and deviate the propagation of SBs increasing the stress necessary for plastic deformation [36]. A second factor to be considered is the large chemical intermixing with the formation of a ZrCuAl phase involving the formation of strong Zr-Al and Cu-Al bonds and by creating short range order Al-centered polyhedral clustered structures, providing high strength as well as a delay to the propagation of SBs [13, 37]. To sum up, the formation of the ZrCuAl phase and the ultrafine nanolayered structure reinforces the mechanical properties of the Al layers, that normally would have *E* and *H* equal to 69 GPa and 1.5 Gpa respectively [38], preventing the drop in mechanical properties usually associated with crystalline/amorphous multilayers.

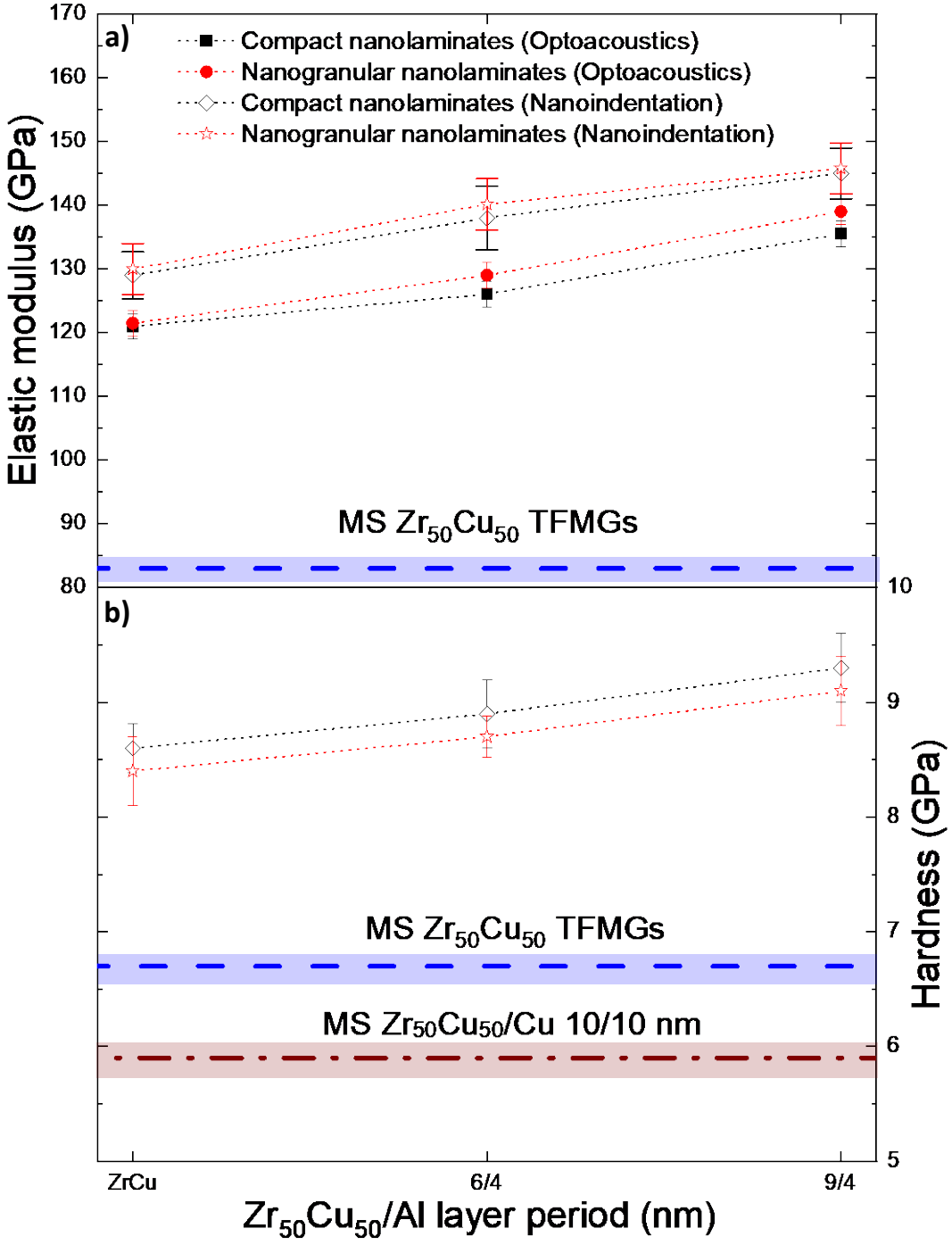

Figure 4. *Evolution of elastic modulus (a) and hardness (b) of compact and nanogranular $Zr_{50}Cu_{50}$/Al U-NLs for different U-NLs configurations. Data are compared with traditional MS ZrCu and ZrCu/Cu multilayers.*

Micropillar compression tests were carried out on both compact and nanogranular $Zr_{50}Cu_{50}$/Al 9/4 nm U-NLs which had the highest density and *H* (Figs. 3,4), thus expecting higher plasticity. Moreover, the higher fraction of ZrCu (vs the $Zr_{50}Cu_{50}$/Al 9/4 U-NLs) is expected to provide enhanced mechanical size effects [8], while the crystalline Al is expected to have beneficial SB booking effects. For the compact U-NLs, Figure 5a shows that after the elastic behavior up to 3.3 %, the stress-strain curve is interrupted by the propagation of the first SB (the full curve up to 15 % strain and the statistics of yield strength and homogeneous deformation are reported in the Section S5 of the supplementary). The yield stress (σ_y) is equal to 3.60 ± 0.08 GPa which is 1.1 GPa higher than of MS-deposited ZrCu homogenous TFMGs and of ZrCu amorphous/crystalline multilayers [9, 39], due to the high mass density of the PLD U-NLs, significant chemical intermixing and the high density of crystalline/amorphous interfaces [24]. The first SB starts to appear at 3.60 ± 0.22 % strain, a value significantly larger than the monolithic TFMG threshold which is usually around 2% [40, 41]. This improvement of plasticity is connected to the presence of Al layers which confine and block the SBs in the amorphous ones promoting a more homogenous deformation. This is confirmed in Figures 5b,c reporting the post-mortem SEM and TEM images of the pillar, highlighting the SB blocking effect of Al-rich layers, while showing the nanoscale periodicity of the Al and $Zr_{50}Cu_{50}$ layers (Figure 5d). The formation of through-the-specimen percolative SBs occurring in U-NL is also expected since the t_a/t_c (thickness of amorphous layer/thickness of crystalline layer) ratio >1, showing a dominant fraction of amorphous sublayers. As a matter of facts, molecular dynamic simulations show that if $t_a/t_c > 1$ the deformation by nucleation and propagation of SB is predominant with respect to the grain boundary and dislocation plasticity of crystalline sublayer [12]. For this reason, the compact U-NLs fail mainly by shear banding, while the chemical heterogeneities and high density of interfaces can only block and delay the SBs propagation thanks to the difference in mechanical properties between the sublayers thus increasing the yield strength and providing only a limited increase of the plasticity with respect monolithic TFMGs (a value which is however ~40% higher) [42].

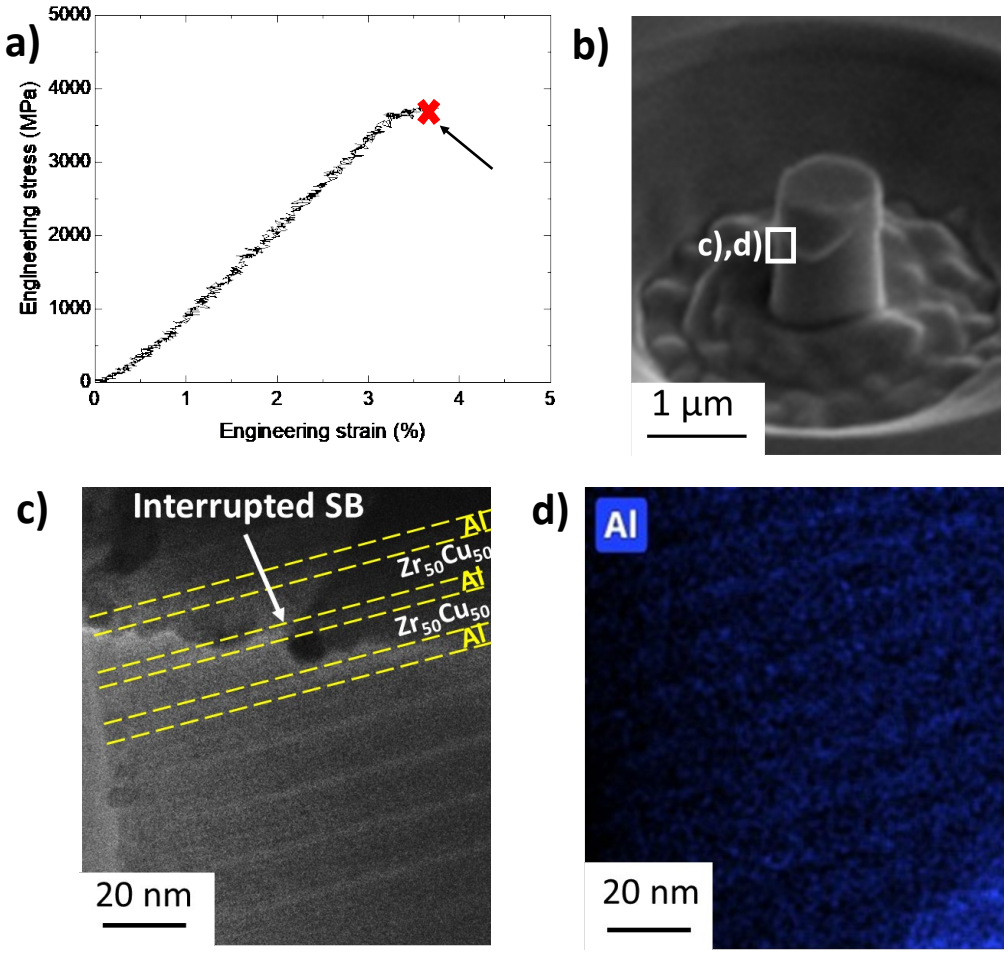

Figure 5. *(a) Engineering stress vs engineering strain curve of compact $Zr_{50}Cu_{50}$/Al 9/4 nm U-NLs with a black arrow highlighting the formation of the first SB causing brittle failure. (b, c, d) Postmortem SEM, TEM and EDX-STEM cross-section of the micropillar showing preliminary SB blocking at Al layers.*

In Figure 6 we show a representative stress-strain curve from a compression of the nanogranular $Zr_{50}Cu_{50}$/Al 9/4 nm U-NLs and corresponding post-mortem SEM and TEM images (the raw curve and statistics of yield strength and homogeneous deformation are in the Section S5 of the supplementary). The stress increases linearly up to 2.5 % deformation upon which the pillar yields with a σ_y ~3.40 ± 0.06 GPa, a value slightly below the compact counterpart (Figure 5) and in agreement with the trend of hardness (Figure 4b) and related to the higher amount of free volume of cluster-assembled U-NLs which activates plastic deformation at lower stresses and strains with respect to the more ordered compact U-

NLs [43, 44] . However, the nanogranular U-NLs show homogenous deformation up to 6.00 ± 0.36 % and then SB start to appear on the surface of the pillar as revealed by TEM observation (Fig. 6c). However, this event is not followed by a percolation even at larger deformations (>15%), as shown in Figure 6b,c in which only some superficial shear band events are found. This phenomenon is similar to the one observed in nanoglasses in the literature [6, 17] in which the large amount of free volume between amorphous clusters prevents the percolation of embryonic SB in a single major event such as in traditional MGs [43, 44], while favoring a pseudo-homogenous deformation of the specimen through the propagation of fine SBs which are confined in the external surface [6]. Another class of nanolaminates which show a similar deformation mechanism are the CoCrNi/TiZrNbHf 18/12 nm crystalline/amorphous multilayers which could achieve σ_y ~3.6 GPa and large deformations with non-percolative cracking events similar to nanogranular U-NLs (Figure 6) due to the high density of interfaces and chemical partitioning between the two sublayers, managing to block crack percolation [45].

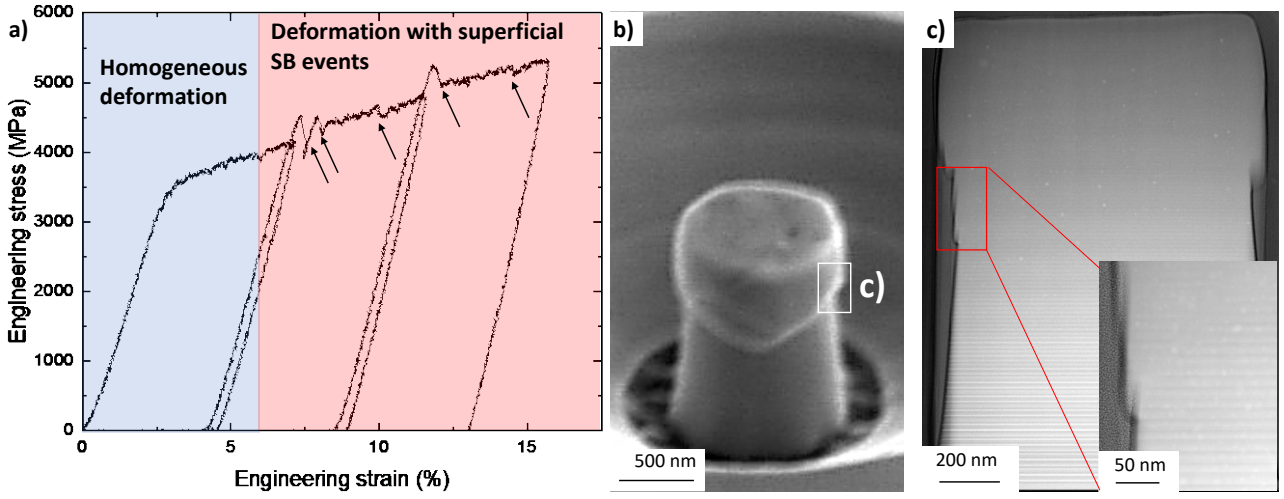

Figure 6. *(a) Engineering stress-strain curve of nanogranular $Zr_{50}Cu_{50}$/Al 9/4 nm U-NLs highlighting the different deformation regimes (homogeneous and plastic with superficial SB events underlined by black arrows). (b,c) Post-mortem SEM image of the micropillar and HAADF-STEM cross-section highlighting superficial non-percolative shear bands.*

Figure 7 reports the normalized shear strength τ_y/G (G = shear modulus) vs homogenous deformation for different classes of materials. τ_y is calculated as $\sigma_y/2$ [46] and G is obtained by BLS for the U-NLs (section S3 of the supplementary) or as $E/(2(1+\nu))$, where E is the elastic modulus and ν is the Poisson's ratio from literature data. We compared our data with homogenous TFMGs [40, 41], MS multilayers with a similar bilayer period alternating amorphous/crystalline sublayers [9, 47], fully crystalline metallic NLs [26] and crystalline metal/ceramic NLs [21, 48].

We show that the PLD U-NLs have very high τ_y/G values equal to $37*10^{-3}$ for compact U-NLs and $34*10^{-3}$ for the nanogranular U-NLs, which are roughly half the theoretical strength limit $(1+\nu)/20$ (ν = 0.3-0.4) obtained from the theoretical yield strength σ_{th} equal to $E/20$ for metallic materials [49]. Such values are much higher than those of current MS multilayers and TFMGs thanks to the high mass density related to the high plasma energies of PLD and the fine nanolayered structure, increasing the stress required for the propagation of SBs by adding chemical interfaces between amorphous and crystalline layers with different mechanical properties. These interfaces confine and deviate the SBs developing in the amorphous layers while absorbing the dislocations generated in the crystalline layers. Finally, we can conclude that the nanogranular U-NLs possess the best combination of normalized strength and homogenous deformation thanks to the combination of the inter-layer chemical heterogeneities and the intra-layer density fluctuations related to the cluster assembled growth, preventing the propagation of mature SB events. Most important the high free volume fraction due the cluster-assembled growth and the complex interplay with the local heterogeneities (interfaces and chemical fluctuations), provide the formation of non-percolative SB events which are arrested in the proximity of the surface even at larger deformations >15%. Thus potentially extend the field of applicably of such materials way above MS multilayers.

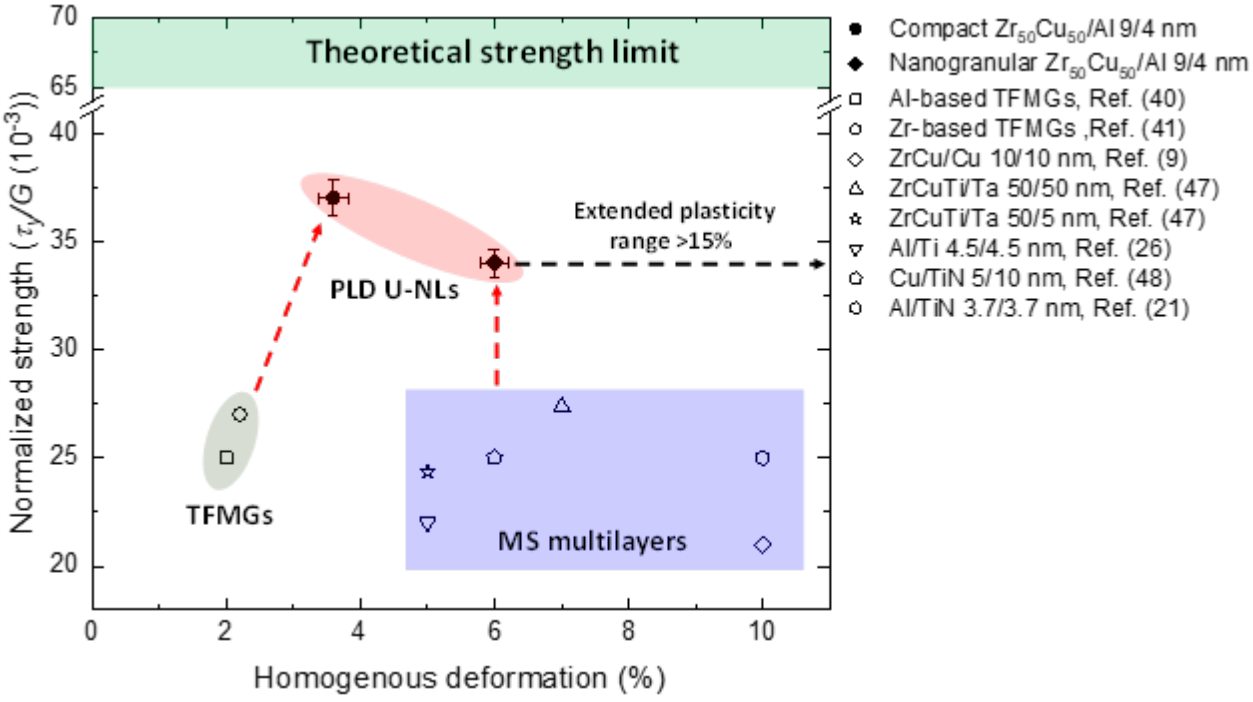

Figure 7. *Map of the normalized strength vs homogenous deformation comparing PLD U-NLs with traditional MGs and crystalline/amorphous multilayers fabricated by magnetron sputtering (MS), as reported in the literature. A black dashed arrow indicates the interval of extended plasticity of the nanogranular U-NLs in which only superficial non-percolative SBs appear.*

4. Conclusions

In this work, we push the limits of pulsed laser deposition (PLD) to develop crystal/glass (Al/$Zr_{50}Cu_{50}$) ultrafine nanolaminates (U-NLs), with controllable nm-scale bilayer period and with tunable (compact and nanogranular) morphology. We show that:

- Both compact and nanogranular U-NLs are characterized by a fine nanolayering with ~4 nm Al layers alternating with 6-9 nm $Zr_{50}Cu_{50}$ layers. This results in a high density of crystalline/amorphous interfaces, coupled with significant interlayer chemical intermixing with the formation of a ZrCuAl phase.

- The mass density of the U-NLs surpasses that of ZrCu/Al sputter-deposited multilayers and monolithic ZrCu metallic glasses, despite the addition of Al (~30-40% vol.). This is attributed to the high kinetic energy of the ablated species during PLD process leading to densification and chemical intermixing promoted by the high out-of-equilibrium conditions.
- The unique microstructure of U-NLs results in significantly enhanced *E* and *H,* reaching up to 139 and 9.3 GPa, respectively. These values surpass by 30% those reported in the literature counterparts due to the presence of a high density of nanointerfaces, increased mass density and the formation of a ZrCuAl phase, enhancing the stress necessary for SB propagation and the mechanical properties.
- Micropillar compression tests reveal that compact U-NLs exhibit the highest yield strength (σ_y) ~3.6 GPa. However, the deformation involves the propagation of SBs which are partially mitigated by the Al-rich layers, resulting in failure >3.6% deformation. In contrast, nanogranular U-NLs have slightly lower σ_y ~3.4 GPa, but their higher free volume content enables them to accommodate more extensive homogenous elasto-plastic deformation without catastrophic failure even for >15% deformations.
- Our PLD-deposited U-NLs demonstrate a superior balance between normalized strength τ_y/G and ductility, surpassing the majority of multilayers and monolithic TFMGs reported in the literature. Additionally, the absence of percolative SBs in nanogranular U-NLs expands their range of applicability, way beyond that of sputter-deposited MLs.

Overall, we demonstrate the effective manipulation of atomic and microstructural heterogeneities within ultrafine crystalline/amorphous ($Al/Zr_{50}Cu_{50}$) nanolaminates as a successful approach to finely tune and enhance the mechanical properties beyond the single-phase constituents and surpassing traditional tread-off between strength and ductility.

Our findings offer crucial insights for the design of new thin films with exceptional mechanical performances capable to resist to intense and complex loading configurations, which are relevant across various application domains such as of microelectronics and structural coatings.

Supporting information

"Additional details regarding the deposition method and characterization techniques including examples of raw data"

Author Contributions

Francesco Bignoli: carried out the PLD deposition, SEM and XRR, optoacoustic and nanoindentation experiments and assisting for micropillar compression. He analyzed all the data and wrote the original draft.

Prof. Gregory Abadias: supervised the XRR characterization.

Dr. Alice Lassnig and Dr. Christoph Gammer: carried out the TEM experiments.

Dr. Ali Ahmadian: carried out the TEM experiments on micropillars after compression.

Camila Aguiar Teixeira: fabricated and compressed the micropillars.

Dr. Subin Lee: supervised the micropillar compression experiments and reviewed the corresponding data.

Prof. Giancarlo Terraneo: carried out the X-ray diffraction.

Prof. Philippe Djemia: supervised optoacoustic characterization.

Profs. Andrea Li Bassi, Damien Faurie and Matteo Ghidelli: supervised the project, finalized the manuscript and secured funding.

Prof. Matteo Ghidelli: conceived, led and coordinate the entire project, co-wrote the manuscript and secured funding.

All the authors contributed to the discussion of the results and approved the final version of the manuscript.

Acknowledgements

M. Ghidelli, A. Li Bassi and D. Faurie acknowledge the financial support of the Université Franco Italienne (UFI) for the funding of the PhD scholarship of F. Bignoli through a Vinci Cap. III Grant (#C3-2286). M. Ghidelli and P. Djemia acknowledge the financial support of ANR-DFG project EGlass (N°ANR-22-CE92-0026-01). C. A. Teixeira, S. Lee and C. Kirchlechner acknowledge the financial support from the Robert-Bosch-Foundation and from the Helmholtz Program Materials Systems Engineering. A. Lassnig acknowledges funding of the Austrian Science Fund (FWF): T891-N36, Y1236-N37.

References

(1) Ashby, M. F.; Greer, A. L. Metallic glasses as structural materials. *Scripta Materialia* **2006**, *54* (3), 5. DOI: https://doi.org/10.1016/j.scriptamat.2005.09.051.

(2) Greer, A.; Cheng, Y.; Ma, E. Shear bands in metallic glasses. *Materials Science and Engineering: R: Reports* **2013**, *74* (4), 71-132.

(3) Nomoto, K.; Ceguerra, A. V.; Gammer, C.; Li, B.; Bilal, H.; Hohenwarter, A.; Gludovatz, B.; Eckert, J.; Ringer, S. P.; Kruzic, J. J. Medium-range order dictates local hardness in bulk metallic glasses. *Mater. Today* **2021**, *44*, 48-57. DOI: https://doi.org/10.1016/j.mattod.2020.10.032.

(4) Nomoto, K.; Li, B.; Gammer, C.; Ceguerra, A. V.; Bilal, H.; Hohenwarter, A.; Eckert, J.; Gludovatz, B.; Ringer, S. P.; Kruzic, J. J. Deformation-induced medium-range order changes in bulk metallic glasses. *Phys. Rev. Mater.* **2022**, *6* (4), 043603. DOI: 10.1103/PhysRevMaterials.6.043603.

(5) Ivanisenko, Y.; Kübel, C.; Nandam, S. H.; Wang, C.; Mu, X.; Adjaoud, O.; Albe, K.; Hahn, H. Structure and properties of nanoglasses. *Adv. Eng. Mater.* **2018**, *20* (12), 1800404.

(6) Nandam, S. H.; Schwaiger, R.; Kobler, A.; Kübel, C.; Wang, C.; Ivanisenko, Y.; Hahn, H. Controlling shear band instability by nanoscale heterogeneities in metallic nanoglasses. *J. Mater. Res.* **2021**, *36* (14), 2903-2914.

(7) Ghidelli, M.; Orekhov, A.; Li Bassi, A.; Terraneo, G.; Djemia, P.; Abadias, G.; Nord, M.; Béché, A.; Gauquelin, N.; Verbeeck, J.; Raskin J. P.; Schryvers, D.; Pardoen T.; Idrissi H. Novel class of nanostructured metallic glass films with superior and tunable mechanical properties. *Acta Mater.* **2021**, *213*, 116955.

(8) Ghidelli, M.; Idrissi, H.; Gravier, S.; Blandin, J.-J.; Raskin, J.-P.; Schryvers, D.; Pardoen, T. Homogeneous flow and size dependent mechanical behavior in highly ductile Zr65Ni35 metallic glass films. *Acta Mater.* **2017**, *131*, 246-259. DOI: 10.1016/j.actamat.2017.03.072.

(9) Zhang, J.; Liu, G.; Lei, S.; Niu, J.; Sun, J. Transition from homogeneous-like to shear-band deformation in nanolayered crystalline Cu/amorphous Cu–Zr micropillars: Intrinsic vs. extrinsic size effect. *Acta Mater.* **2012**, *60* (20), 7183-7196.
(10) Guo, W.; Jägle, E.; Yao, J.; Maier, V.; Korte-Kerzel, S.; Schneider, J. M.; Raabe, D. Intrinsic and extrinsic size effects in the deformation of amorphous CuZr/nanocrystalline Cu nanolaminates. *Acta Mater.* **2014**, *80*, 94-106. DOI: https://doi.org/10.1016/j.actamat.2014.07.027.
(11) Nasim, M.; Li, Y.; Wen, C. Length-scale dependent deformation, strengthening, and ductility of fcc/fcc Ni/Al nanolaminates using micropillar compression testing. *Acta Mater.* **2020**, *193*, 318-328.
(12) Cheng, B.; Trelewicz, J. R. Design of crystalline-amorphous nanolaminates using deformation mechanism maps. *Acta Mater.* **2018**, *153*, 314-326.
(13) Poltronieri, C.; Brognara, A.; Bignoli, F.; Evertz, S.; Djemia, P.; Faurie, D.; Challali, F.; Li, C.; Belliard, L.; Dehm, G.; Best, J. P.; Ghidelli, M. Mechanical properties and thermal stability of ZrCuAlx thin film metallic glasses: Experiments and first-principle calculations. *Acta Mater.* **2023**, *258*, 119226.
(14) Brognara, A.; Best, J. P.; Djemia, P.; Faurie, D.; Dehm, G.; Ghidelli, M. Effect of composition and nanostructure on the mechanical properties and thermal stability of Zr100-xCux thin film metallic glasses. *Mater. Design* **2022**, *219*, 110752. DOI: https://doi.org/10.1016/j.matdes.2022.110752.
(15) Oliver, W. C.; Pharr, G. M. An improved technique for determining hardness and elastic modulus using load and displacement sensing indentation experiments. *J. Mater. Res.* **2011**, *7* (6), 1564-1583. DOI: 10.1557/JMR.1992.1564 From Cambridge University Press Cambridge Core.
(16) Guo, H.; Yan, P. F.; Wang, Y. B.; Tan, J.; Zhang, Z. F.; Sui, M. L.; Ma, E. Tensile ductility and necking of metallic glass. *Nat. Mater.* **2007**, *6* (10), 735-739. DOI: 10.1038/nmat1984.
(17) Wang, X.; Jiang, F.; Hahn, H.; Li, J.; Gleiter, H.; Sun, J.; Fang, J. Sample size effects on strength and deformation mechanism of Sc75Fe25 nanoglass and metallic glass. *Scripta Mater.* **2016**, *116*, 95-99.
(18) Ghidelli, M.; Gravier, S.; Blandin, J.-J.; Raskin, J.-P.; Lani, F.; Pardoen, T. Size-dependent failure mechanisms in ZrNi thin metallic glass films. *Scripta Mater.* **2014**, (89), 4.
(19) Nandam, S. H.; Ivanisenko, Y.; Schwaiger, R.; Śniadecki, Z.; Mu, X.; Wang, D.; Chellali, R.; Boll, T.; Kilmametov, A.; Bergfeldt, T. Cu-Zr nanoglasses: Atomic structure, thermal stability and indentation properties. *Acta Mater.* **2017**, *136*, 181-189.
(20) Chen, Z. Q.; Li, M. C.; Cao, J. S.; Li, F. C.; Guo, S. W.; Sun, B. A.; Ke, H. B.; Wang, W. H. Interface dominated deformation transition from inhomogeneous to apparent homogeneous mode in amorphous/amorphous nanolaminates. *J. Mater. Sci. Technol.* **2022**, *99*, 178-183. DOI: https://doi.org/10.1016/j.jmst.2021.04.073.
(21) Bhattacharyya, D.; Mara, N.; Dickerson, P.; Hoagland, R.; Misra, A. Compressive flow behavior of Al–TiN multilayers at nanometer scale layer thickness. *Acta Mater.* **2011**, *59* (10), 3804-3816.
(22) Aziz, M. J. Film growth mechanisms in pulsed laser deposition. *Appl. Phys. A* **2008**, *93*, 579-587.
(23) Takeuchi, A.; Inoue, A. Classification of bulk metallic glasses by atomic size difference, heat of mixing and period of constituent elements and its application to characterization of the main alloying element. *Mater. Trans.* **2005**, *46* (12), 2817-2829.
(24) Cui, Y.; Huang, P.; Wang, F.; Lu, T.; Xu, K. The hardness and related deformation mechanisms in nanoscale crystalline–amorphous multilayers. *Thin solid films* **2015**, *584*, 270-276.
(25) Schuh, C. A.; Lu, K. Stability of nanocrystalline metals: The role of grain-boundary chemistry and structure. *Mrs Bull.* **2021**, *46*, 225-235.
(26) Zhang, Y.; Su, R.; Niu, T.; Richter, N.; Xue, S.; Li, Q.; Ding, J.; Yang, B.; Wang, H.; Zhang, X. Thermal stability and deformability of annealed nanotwinned Al/Ti multilayers. *Scripta Mater.* **2020**, *186*, 219-224.
(27) Yu, P.; Bai, H. Y. Poisson's ratio and plasticity in CuZrAl bulk metallic glasses. *Mater. Sci. Eng. A* **2008**, *485* (1-2), 1-4. DOI: 10.1016/j.msea.2007.07.062.
(28) Afonso, C. N.; Gonzalo, J. Pulsed laser deposition of thin films for optical applications. *Nucl. Instrum. Meth. B* **1996**, *116* (1-4), 404-409.

(29) Apakina, V.; Karuzskii, A.; Kogan, M.; Kvit, A.; Melnik, N.; Mityagin, Y. A.; Murzin, V.; Orlikovsky, A.; Perestoronin, A.; Tkachenko, S. Studies of nanoscale structure and its transformation in pulsed-laser deposited dense diamond-like carbon films. *Diam. Relat. Mater.* **1997**, *6* (5-7), 564-568.
(30) Anderson, K.; Weritz, J.; Kaufman, J. G. 1xxx Aluminum Alloy Datasheets. *Properties and Selection of Aluminum Alloys. ASM Handbooks, ASM International* **2019**, *2B*, 1.
(31) Oliver, W. C.; Pharr, G. M. Measurement of hardness and elastic modulus by instrumented indentation: Advances in understanding and refinements to methodology. *J. Mater. Res.* **2004**, *19* (1), 3-20.
(32) M. Apreutesei; P. Steyer; L. Joly-Pottuz; A. Billard; J. Qiao; S. Cardinal; F. Sanchette; J.M. Pelletier; Esnouf, C. Microstructural, thermal and mechanical behavior of co-sputtered binary Zr–Cu thin film metallic glasses. *Thin solid films* **2014**, (561), 7. DOI: http://dx.doi.org/10.1016/j.tsf.2013.05.177.
(33) Besozzi, E.; Dellasega, D.; Pezzoli, A.; Conti, C.; Passoni, M.; Beghi, M. Amorphous, ultra-nano-and nano-crystalline tungsten-based coatings grown by Pulsed Laser Deposition: mechanical characterization by Surface Brillouin Spectroscopy. *Mater. Design* **2016**, *106*, 14-21.
(34) Besozzi, E.; Dellasega, D.; Russo, V.; Conti, C.; Passoni, M.; Beghi, M. G. Thermomechanical properties of amorphous metallic tungsten-oxygen and tungsten-oxide coatings. *Mater. Design* **2019**, *165*, 107565. DOI: 10.1016/j.matdes.2018.107565.
(35) Xue, F.; Huang, P.; Liu, M.; Xu, K.; Wang, F.; Lu, T. Unusual strain rate sensitivity of nanoscale amorphous CuZr/crystalline Cu multilayers. *Mater. Sci. Eng. A* **2017**, *684*, 84-89.
(36) Kuan, S.; Du, X.; Chou, H.; Huang, J. Mechanical response of amorphous ZrCuTi/PdCuSi nanolaminates under nanoindentation. *Surf. Coat. Tech.* **2011**, *206* (6), 1116-1119.
(37) Das, J.; Tang, M. B.; Kim, K. B.; Theissmann, R.; Baier, F.; Wang, W. H.; Eckert, J. "Work-hardenable" ductile bulk metallic glass. *Phys. Rev. Lett.* **2005**, *94* (20), 205501.
(38) Farhat, Z.; Ding, Y.; Northwood, D.; Alpas, A. Effect of grain size on friction and wear of nanocrystalline aluminum. *Mater. Sci. Eng. A* **1996**, *206* (2), 302-313.
(39) Liu, M.; Du, X.; Lin, I.; Pei, H.; Huang, J. Superplastic-like deformation in metallic amorphous/crystalline nanolayered micropillars. *Intermetallics* **2012**, *30*, 30-34.
(40) Wu, G.; Liu, C.; Sun, L.; Wang, Q.; Sun, B.; Han, B.; Kai, J.-J.; Luan, J.; Liu, C. T.; Cao, K. Hierarchical nanostructured aluminum alloy with ultrahigh strength and large plasticity. *Nat. Commun.* **2019**, *10* (1), 5099.
(41) Ye, J.; Chu, J.; Chen, Y.; Wang, Q.; Yang, Y. Hardness, yield strength, and plastic flow in thin film metallic-glass. *J. Appl. Phys.* **2012**, *112* (5).
(42) Wu, G.; Chan, K.-C.; Zhu, L.; Sun, L.; Lu, J. Dual-phase nanostructuring as a route to high-strength magnesium alloys. *Nature* **2017**, *545* (7652), 80-83.
(43) Ritter, Y.; Şopu, D.; Gleiter, H.; Albe, K. Structure, stability and mechanical properties of internal interfaces in Cu64Zr36 nanoglasses studied by MD simulations. *Acta Mater.* **2011**, *59* (17), 6588-6593.
(44) Şopu, D.; Ritter, Y.; Gleiter, H.; Albe, K. Deformation behavior of bulk and nanostructured metallic glasses studied via molecular dynamics simulations. *Phys. Rev. B* **2011**, *83* (10), 100202.
(45) Wu, G.; Liu, C.; Brognara, A.; Ghidelli, M.; Bao, Y.; Liu, S.; Wu, X.; Xia, W.; Zhao, H.; Rao, J. Symbiotic crystal-glass alloys via dynamic chemical partitioning. *Mater. Today* **2021**, *51*, 6-14.
(46) Johnson, W.; Samwer, K. A universal criterion for plastic yielding of metallic glasses with a (T/T g) 2/3 temperature dependence. *Phys. Rev. Lett.* **2005**, *95* (19), 195501.
(47) Chou, H.; Du, X.; Lee, C.; Huang, J. Enhanced mechanical properties of multilayered micropillars of amorphous ZrCuTi and nanocrystalline Ta layers. *Intermetallics* **2011**, *19* (7), 1047-1051.
(48) Raghavan, R.; Wheeler, J.; Esqué-De los Ojos, D.; Thomas, K.; Almandoz, E.; Fuentes, G.; Michler, J. Mechanical behavior of Cu/TiN multilayers at ambient and elevated temperatures: Stress-assisted diffusion of Cu. *Mater. Sci. Eng. A* **2015**, *620*, 375-382.
(49) Ashby, M.; Greer, A. L. Metallic glasses as structural materials. *Scripta Mater.* **2006**, *54* (3), 321-326.

Table Of Contents (TOC)